In Vivo Determination of Intra-Myocellular Lipids in Human Muscle by Means of Localized ^{1}H-MR-Spectroscopy

Chris Boesch, Johannes Slotboom, Hans Hoppeler, Roland Kreis

Intra-myocellular lipids (IMCL) are stored in droplets in the cytoplasm of muscle cells and are an energy storage form readily accessed during long-term exercise. ^{1}H-MR spectroscopy methods are presented for noninvasive determination of IMCL in human muscle. This is based on (a) the separation of two resonances in the lipid-CH_2-region, with the one assigned to IMCL being independent of muscle orientation relative to the magnetic field and (b) the fact that IMCL resonances scale along with signal amplitudes of metabolites in the muscle cell (e.g., creatine) when voxel size is increased, while lipid signals of bulk fat show a disproportionate growth. Inter-individual and intra-individual reproducibility studies indicate that the error of the method is about 6% and that IMCL levels differ significantly between identical muscles in different subjects, as well as intra-individually when measured at 1 week intervals. IMCL determinations in a single subject before and after strenuous exercise indicate that lipid stores recover with a $t_{1/2}$ of about 1 day.

Key words: proton spectroscopy; skeletal muscle; lipids; substrate.

INTRODUCTION

MR spectroscopy (MRS) has been applied successfully to human muscle *in vivo* ever since magnets of an appropriate bore size became available. However, most of the research was aimed at short-term muscle energy metabolism (1–4) and used either ^{31}P-MRS for the observation of high-energy phosphates or ^{13}C-MRS to investigate muscular glycogen (5).

Water suppressed ^{1}H-MR spectra of human muscle were presumed to feature few metabolite peaks dominated by a large hump of lipid resonances (6–10). When Schick *et al.* (11) compared the lipid resonances in calf muscle and in fat tissue, they observed two compartments of triglycerids with a resonance frequency shift of 0.2 ppm. The authors assigned the resonance at 1.5 ppm to the CH_2-protons of lipids in fat cells and supposed that the shifted resonance at 1.3 ppm could be attributed to lipids located inside muscle cells (i.e., in their cytoplasm), experiencing different bulk susceptibility.

Lipids are either stored as subcutaneous or interstitial adipose tissue (here summarized as extra-myocellular lipids, EMCL) or as intra-myocellular lipids (IMCL) in the form of liquid droplets in the cytoplasm of muscle cells, while free or protein-bound lipids in cytoplasm are of lower concentration. Fatty acids in the converted form of triacylglycerols are the most abundant long-term energy store of the human body. While EMCL (i.e., fat tissue) is metabolically relatively inert, there is evidence that IMCL can be mobilized and utilized with turnover times of several hours (12). IMCL droplets are located in the cytoplasm in contact with mitochondria (13) and provide an important share of the energy supply during long-term endurance activities (14, 15). With regard to availability for cellular oxidation, IMCL are comparable with glycogen, which can be quantified by ^{13}C-MRS (5, 16).

Carefully respecting the anatomical conditions, including fiber orientation in individual human muscles, we were able to demonstrate the angular dependence of two dipolar-coupled resonances X_1 and X_2 centered at 3.93 ppm (17) which later have been characterized as the methylene protons of creatine (Cr) (18). In the same experiments, it was observed that also the chemical shifts of some of the lipid resonances are orientation-dependent (19). In this context it is crucial to distinguish clearly between orientational effects due to dipolar coupling (as for Cr, (17)) and those based on anisotropic susceptibility (as observed for lipid layers). The latter effect will be explored in this manuscript.

Quantitation of IMCL in human muscle by means of ^{1}H-MRS, along with ^{13}C-MRS determination of glycogen, would allow for the noninvasive observation of the complete pattern of intra-cellular substrate storage and use in human muscle in pathology or during sports activities. The present study aimed at: (a) optimizing the separation of IMCL from EMCL, (b) characterizing and assigning the IMCL resonances, (c) developing a theoretical framework for the observed phenomena, (d) estimating the methodological errors and the reproducibility of IMCL determinations, and (e) testing the method in a preliminary recovery experiment after long-term exercise.

MRM 37:484–493 (1997)

From the Department of MR-Spectroscopy and Methodology (C.B., J.S., R.K.), and the Department of Anatomy (H.H.), University of Bern, Bern, Switzerland.

Address correspondence to: Chris Boesch, M.D., Ph.D., Department MR-Spectroscopy and Methodology, MR-Zentrum 1, University and Inselspital, CH-3010 Bern, Switzerland.

Received June 28, 1996; revised October 3, 1996; accepted October 15, 1996.

This work was funded by the Swiss National Foundation 31-30971.91 (to C.B.), 3100-042162.94 (to C.B.), and 3100-42449.94 (to H.H.).

0740-3194/97 $3.00

MATERIAL AND METHODS

Volunteers

All subjects gave their informed consent before the investigation. The series of spectra with rotation of the leg relative to the external field were obtained in *M. tibialis anterior* of a healthy volunteer (32 years, female) laying on her side. The series of spectra with increasing volumes were recorded in *M. tibialis anterior* of a lean volunteer (30 years, male). For the determination of intra-individual and inter-individual reproducibility, subjects with average sportive activity were measured three consecutive times with a break of about 10 min. Between these repetitions, the volunteers left the magnet to make new positioning necessary. For inter-individual reproducibility, 7 volunteers (31.4 ± 6.6 years, 3 female, 4 males) were compared, each subject measured in triplicate. For intra-individual reproducibility, one subject (24 years, female) was measured on 5 different days, 1 week apart and also in triplicate each day as described above. Before Days 2 and 5, this volunteer was asked to hike for 3 h at normal speed. For the determination of IMCL recovery after heavy workload, a 27-year-old male subject performed a 3 h of an intense training bout on his mountain bike (approximately his ordinary training effort, i.e., some 70% of VO_2max). Spectra were obtained pre-exercise, continuously 1 to 3 h after termination of exercise, and subsequently at 6, 8, 21, 28, 53, and 100 h post-workload. For comparison of IMCL levels in different muscle groups, spectra of the soleus and the gastrocnemius muscle were measured within the same session in eight volunteers (age 29 ± 3 years, all male).

MR

MR images for localization and ^{1}H-MR spectroscopy were done on a SIGNA 1.5 Tesla MR system (General Electric, Milwaukee, WI). With the exception of the rotation study, where the body coil was applied for transmission and a 13-cm surface coil for detection, a standard coil for extremities (linear polarized volume coil, diameter 17 cm, length 29 cm) was used. All measurements were performed in *M. tibialis anterior* except for the comparison of soleus and gastrocnemius muscle. Imaging parameters were chosen for optimal separation of the muscles and fasciae (gradient-echo-sequence, 30° flip angle, *TR* 100 ms, *TE* 6.8 ms). For single voxel spectroscopy, an optimized PRESS sequence (20) with *TE* 20 ms, *TR* 3000 ms, 128 acquisitions, 16 phase rotation steps (21), water presaturation, and outer volume suppression was used. To study the angular dependence, at each angle, new images for localization were made, shimming and water-suppression were adjusted, and a PRESS image of the voxel was acquired. However, absolute reproducibility of the voxel content was not possible because the voxel remained aligned parallel to the main axes of the magnet (no oblique voxels). Typical voxel dimensions were $12 \times 11 \times 18$ mm^3 for the reproducibility and the recovery study. The series of spectra from increasing volumes were recorded from nominal voxels of 1.76, 2.27, 2.77, 3.02, 3.28, 3.78 cm^3, obtained by stepwise enlargement of the anteroposterior voxel length at a fixed location. Voxel position for this series was chosen in the corresponding T_1-weighted images such that the smallest voxel did not contain any visible interstitial tissue or fat, while the largest voxel was close to the subcutaneous fat layer. Position and size of the voxels used in the reproducibility and the recovery study were chosen carefully in a scout image to avoid contamination from EMCL (Fig. 1). Voxel positions were calculated for the resonance frequency of creatine-methyl groups (i.e., center frequency at 3.02 ppm). Variations of the voxel size were achieved by modification of the gradient strength. The chemical shift artifact between water and lipid methylenes was 17% of the voxel dimension defined by the PRESS sequence in anteroposterior and superior-inferior direction and 9% in right-left direction, compared with 3 mm in the imaging sequences used.

Fitting of Spectra

H_2O signal amplitude was determined from a fit of the first points in a series of FIDs obtained without water suppression. For the study with increasing voxel size, areas were determined by a Marquart-fit of Lorentz-lines, using a standard analysis package (SAGE, General Electric, Milwaukee, WI). A sum of the areas of six resonances from 4.2 to 2.7 ppm, including resonances from Cr and trimethylamines (TMA), was defined as metabolite signal (M). Cr levels were estimated from the CH_3 peak at 3.02 ppm.

To obtain a better estimation of the areas for the reproducibility and recovery studies, an improved version of a vector-based nonlinear least-squares complex frequency domain fitting algorithm was applied (22, 23). This fit uses time domain model signals for the quantification of the water suppressed proton spectra, allowing for a mixed lineshape fit and the incorporation of prior knowledge.

Figure 2 shows how difference spectroscopy reveals almost clean spectra of either pure IMCL or EMCL. A subtraction of mixed spectra with appropriate multiplication of the individual spectra allows cancellation of

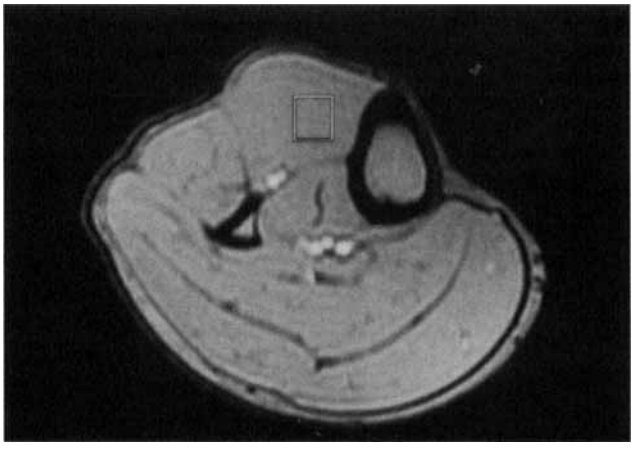

FIG. 1. Axial image for localization through the calf of a 27-year-old male volunteer. A voxel of typical size and position is indicated in *M. tibialis anterior*. Voxels were positioned carefully to avoid contamination by EMCL. Sequence parameters of images for localization: gradient echo, 30° flip angle, *TR* 100 ms, *TE* 6.8 ms, slice thickness 5 mm.

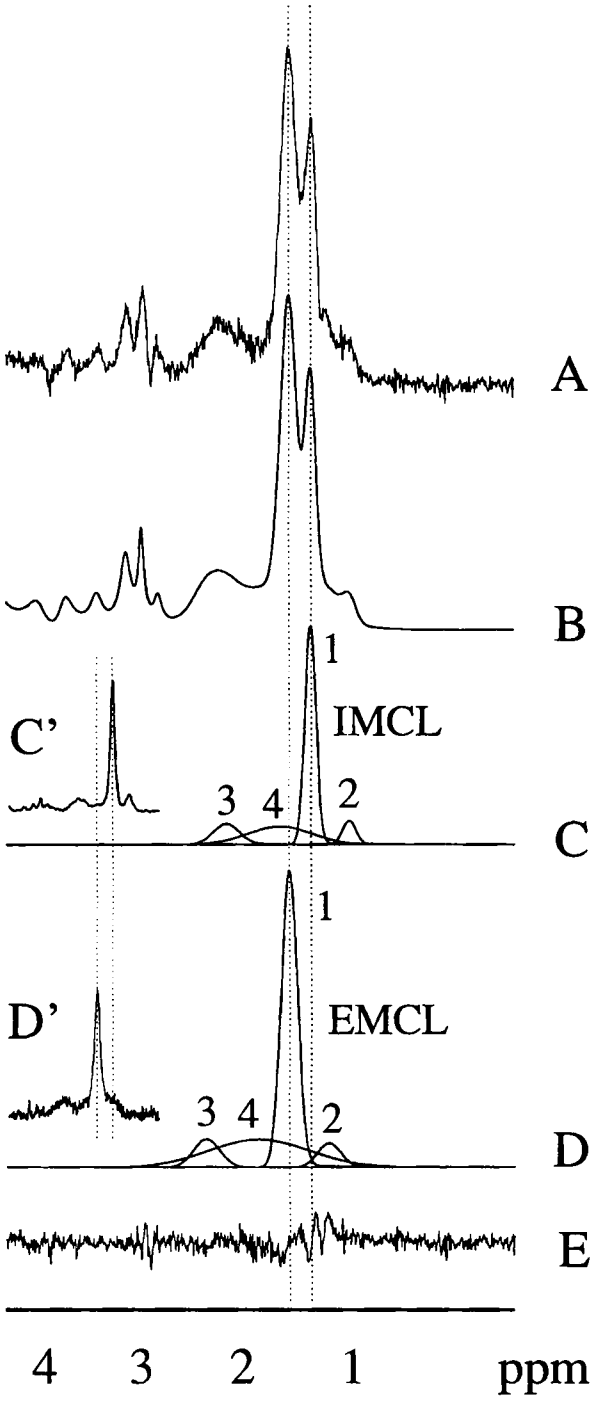

FIG. 2. ^{1}H-MR spectra of *M. tibialis anterior* and fitted data. Trace A contains a typical experimental spectrum obtained from *M. tibialis anterior* with the corresponding fitted spectrum in Trace B. The fit is based on Lorentzian line shapes for the metabolite part (2.7–4.3 ppm) and Gaussian line shapes for IMCL and EMCL. The latter moieties are both plotted separately and decomposed into its four constituent components in Traces C and D, respectively. Difference spectra (C',D') had been obtained from spectra with different ratios of IMCL and EMCL. By appropriate scaling, IMCL and EMCL signals, respectively, were nulled and "pure" spectra of the remaining component were available to provide spectra from which prior knowledge for the fitting procedure could be extracted (peak area ratios and differences of linewidths and chemical shifts of the constituent signals). The residuals of fitting the spectrum in A are shown in Trace E.

one of the contributions. With the aid of such difference spectra, prior knowledge was obtained for the strongly overlapping resonances of EMCL and IMCL. Seven resonances between 2.7 and 4.3 ppm from different metabolites and the residual water peak were fitted with a complex Lorentzian lineshape model. The IMCL and EMCL parts of the spectra were estimated concurrently with a complex Gaussian lineshape model. The use of Gaussian lineshape is motivated by the fact that lipid resonances consist of a mixture of similar but not identical chemical species (e.g., variations in chain length) leading to a distribution of chemical shifts within one resonance. The errors in the estimated lineshape model parameters were calculated after the fit by evaluating the diagonal elements of the covariance matrix. Areas, resonance frequencies, and linewidth parameters of all metabolite peaks (i.e., 2.7–4.3 ppm) were modeled independently from each other. Simultaneous zero-order phase variation of all lines – including IMCL and EMCL – was allowed. The lineshape model of IMCL and EMCL consisted of four Gaussian lines each: in addition to the well known resonances from methyl and methylene protons (11), two broad lines were added to take into account the lipid contributions between 1.5 and 2.5 ppm, attributed to various, chemically different methylene protons in esters and adjacent to unsaturated and polyunsaturated bonds of fatty acids (11). Abbreviations were defined as follows: IMCL1 being the methylene resonance at 1.28 ppm; IMCL2, the methyl resonance at 0.885 ppm; IMCL3, a first broad resonance at 2.15 ppm; and IMCL4, the second, even broader component at 1.60 ppm. The resonance positions of the corresponding EMCL lines were 1.49, 1.07, 2.33, and 1.80 ppm for EMCL1 to EMCL4. Some of the line parameters were related by prior knowledge (24), based on the data obtained from difference spectra: Areas, linewidths, and resonance frequencies of IMCL2, IMCL3, and IMCL4 were kept fixed with respect to IMCL1. Areas, linewidths, and resonance frequencies of EMCL2, EMCL3, and EMCL4 were kept fixed with respect to EMCL1, except for areas of EMCL3 and EMCL4, which were fitted without constraint from prior knowledge. The exclusion of EMCL3 and EMCL4 from area constraints is based on the experience that the areas of these lines –which in fact are primarily included in the fit to define the baseline for methyl and methylene proton peaks of IMCL and EMCL –may dominate the area determination of EMCL1 if mutual area constraints are active.

Concentration Units

For conversion to an absolute scale, spectra were divided by the hypothetical signal amplitude of unsuppressed water at $TE = 0$ ms obtained from fitting the signal decay in separate acquisitions with differing *TE*s to an exponential decay (25). As long as the muscle water concentration remains constant, metabolite or lipid concentrations are therefore given in arbitrary units on an absolute scale, however, without conversion to mmols per liter or kg, since no comparison with chemical measurements is presently aimed at. Such a conversion from arbitrary to standard units is possible but will involve further mea-

surements and assumptions. Transverse and longitudinal relaxation times, pulse profiles and calibration constants will have to be determined and a certain IMCL composition has to be assumed. This lipid mixture in droplets can be estimated from free fatty acids in plasma (15), which is composed of roughly 24% palmitic acid, 14% stearic acids, 43% oleic acids, and 10% linoleic acids. The calculated proton density for this lipid mixture (0.108 mol protons/cm^3) is thus very similar for that of water (0.111 mol protons/cm^3).

Electron Microscopy

Electron micrographs of lipid droplets (IMCL; Fig. 3) were obtained from biopsies of human vastus lateralis muscle processed for EM according to established methods (13).

Statistics

A one-way analysis of variance (ANOVA) was performed on inter-individual and intra-individual reproducibility data. Relative errors of the method (i.e., residual coefficients of variance) were determined as the square-root of the residual mean square, i.e., of the variance *within* the groups (26). A fit of the recovery curve was obtained from standard PC based software (Solver, Microsoft Excel 4.0).

RESULTS

Angular Dependence of CH_2 Resonances

Figure 4 shows the angular dependence of the methylene resonances of lipids. One signal at 1.25 ppm is independent of the angle between leg and static magnetic field. A second signal shows a clear shift when the leg is rotated in the field. Note that the line broadens when the leg is perpendicular to the field while it is sharpest with the leg parallel to the magnet. Variations of the signal-amplitude of the shifting signal (EMCL) are observed since the voxel content varies sligthly from experiment to experiment (no oblique voxels used). The simultaneous variations in the splitting of the doublet X1-X2 are due to dipolar coupling of the creatine CH_2 protons (17, 18).

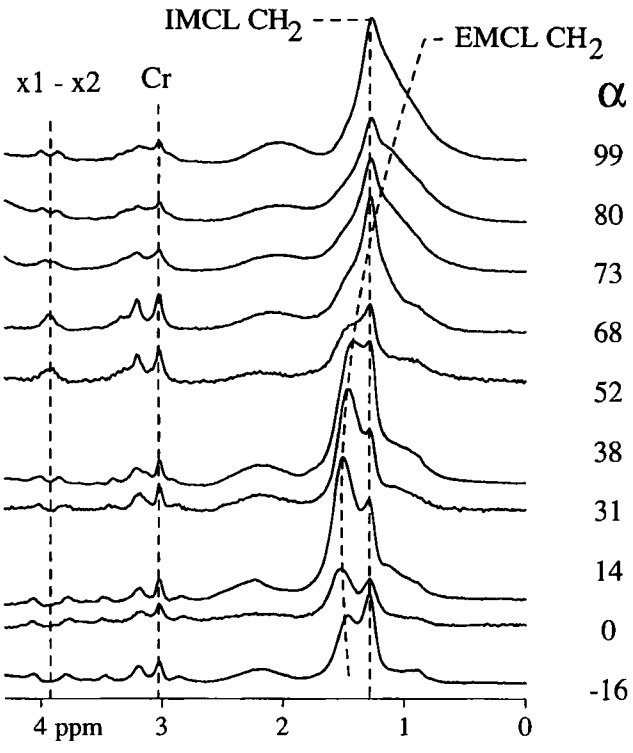

FIG. 4. Series of ^{1}H-MR spectra of *M. tibialis anterior* in a 32 y old female volunteer with her calf at different angles with respect to the static magnetic field. Chemical shift reference is the CH_3-signal of Cr at 3.02 ppm. While one part of the lipid CH_2 signals at 1.25 ppm is constantly visible at all different angles, a second portion of signals shows a variable resonance frequency as well as an angle-dependent broadening of the signal (broken line for illustration only). The amount of the shifting resonance (EMCL) varies considerably since the voxel is aligned along the main axes of the magnet. Best separation between the two signals is achieved when the tibialis muscle is roughly parallel to the static magnetic field. This is consistent with theory (see Appendix). The variable splitting of the X1-X2 doublet is due to dipolar coupling of the CH_2 protons of creatine and is described and analyzed in (17, 18).

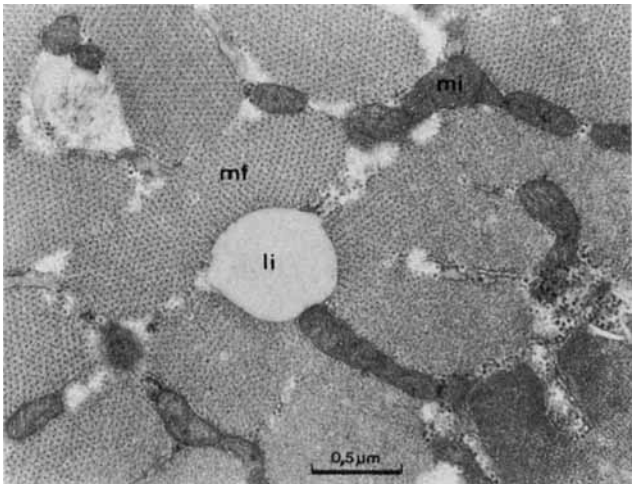

FIG. 3. Cross-section of a portion of a human muscle fiber. An intra-myocellular lipid droplet (*li*) can be seen in close apposition to a mitochondrion (mi). The dimensions of the lipid droplets can be estimated from the scale provided. (mf) denotes myofilaments.

Increasing Voxel Size

The unsuppressed H_2O signal is linearly correlated with the nominal voxel size (r^2 = 0.999). In the water-suppressed spectra (Fig. 5), metabolite (r^2 = 0.996) and Cr (r^2 = 0.994) signals depend linearly on the water signal from within the voxel (Fig. 6). The same is observed for the signal at 1.25 ppm (r^2 = 0.835), which is attributed to IMCL. This signal is also linearly related to the Cr peak area (r^2 = 0.886). None of the correlations featured a significant offset from zero. In contrast, the signal at 1.5 ppm, attributed to EMCL, shows a linear relationship only for small voxel sizes; increasing voxel size leads to a disproportionate increase in signal intensity (Fig. 6). Since the spectra in Fig. 5 are scaled to H_2O, IMCL signal amplitude is independent of voxel size while the signal at 1.5 ppm increases dramatically for larger voxels.

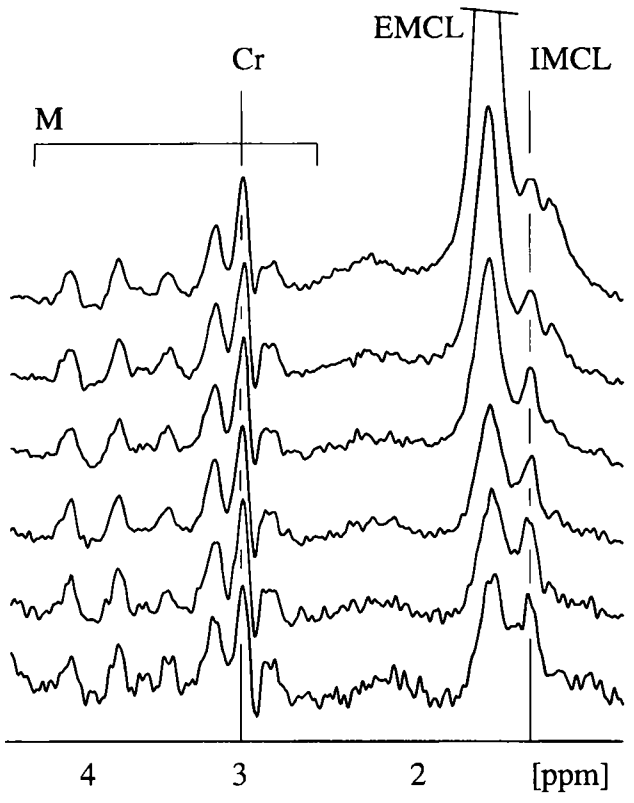

FIG. 5. Series of ^{1}H-MR spectra from *M. tibialis anterior* oriented parallel to the static magnetic field with increasing voxel size (1.76, 2.27, 2.77, 3.02, 3.28, 3.78 cm^3, smallest voxel in the lowest trace) at the same voxel position, scaled by the H_2O signal. The IMCL signal at 1.25 ppm shows constant amplitude throughout the experiment while the EMCL signal at 1.5 ppm features an increasing amplitude at larger voxels, which include more extra-muscular structures such as subcutaneous fat and lipids from fasciae. M denotes total of intra-cellular metabolites.

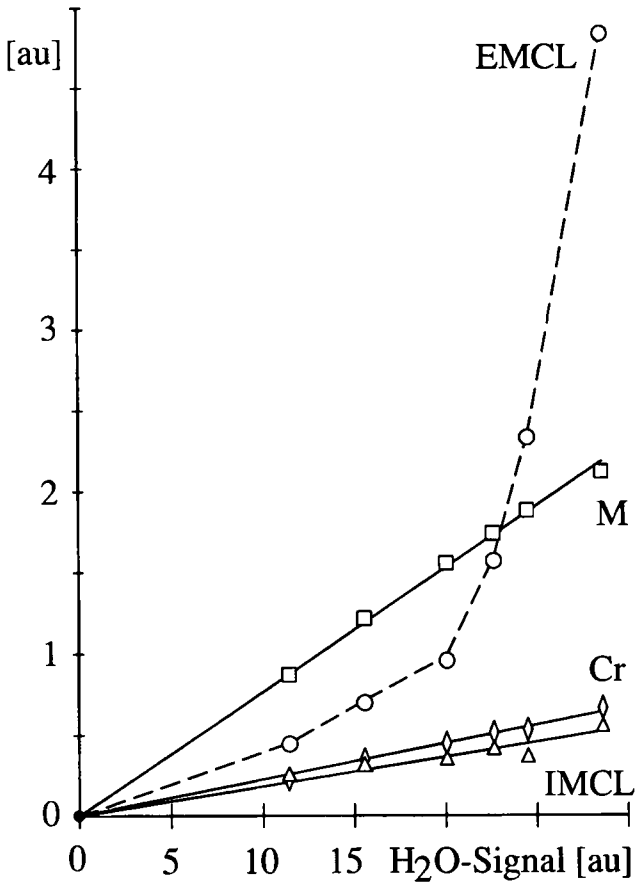

FIG. 6. Signal areas of IMCL (triangles), EMCL (circles), metabolites (M, squares, sum of peaks from 4.2–2.7 ppm) and Cr (CH_3 peak at 3.02 ppm, diamonds) as a function of the unsuppressed water signal. Acquisition parameters as described in Fig. 5. Cr, M, and IMCL scale with the water signal, which represents the muscular tissue within the voxel. The EMCL signal increases steeply and independently of the water signal with larger voxel size (curve shown as dashed line).

Reproducibility

Five sessions with three independent IMCL determinations each and a delay of 1 week between subsequent sessions in a single volunteer (Fig. 7) revealed large differences between the sessions but much less between the repeated measurements under the same conditions, i.e., with repositioning in the magnet after a 5-min break walking around in the magnet room. IMCL levels were visibly lower in Sessions 2 and 5 before which the volunteer had hiked for about 3 h at a convenient pace. An ANOVA test showed (Table 1) highly significant differences ($P \ll 0.001$) between the sessions and a residual relative error of 6.1%. Cr levels were notably stable over the whole period of time (within 3%, no significance for differences between sessions: $P = 0.857$).

Table 1
One-Way Analysis of Variance (ANOVA) for Inter-Individual and Intra-Individual Reproducibility of IMCL Determinations

	Inter-Individual	Intra-Individual
Significance P between groups	$3.5 \cdot 10^{-11}$	$1.8 \cdot 10^{-7}$
Residual coefficient of variance	6.7%	6.1%

Residual coefficients of variance are an upper estimation of the methodological errors and are the square root of the within-group variance (i.e., the residual sum-of-square) (26).

Inter-individual differences of IMCL in seven volunteers (Table 1) were highly significant ($P \ll 0.001$) and are clearly visible in Fig. 8. The residual relative error (coefficient of variance) for inter-individual comparison was 6.7%. Between various subjects, Cr levels differed significantly ($P = 0.004$).

IMCL Levels in Different Muscle Groups

Figure 9 demonstrates obvious differences between IMCL levels in soleus and gastrocnemius muscle in averaged spectra obtained from eight subjects. The resonance at 1.25 ppm which is attributed to IMCL showed very low levels in the gastrocnemius muscle, while it was found to be much higher in the soleus muscle. The amplitude of the EMCL resonance at 1.5 ppm depends on the amount of bulk fat included in the voxel leading to large variations. Figure 9 also documents the orientation-dependence of the other metabolite signals due to dipolar coupling as described earlier (17).

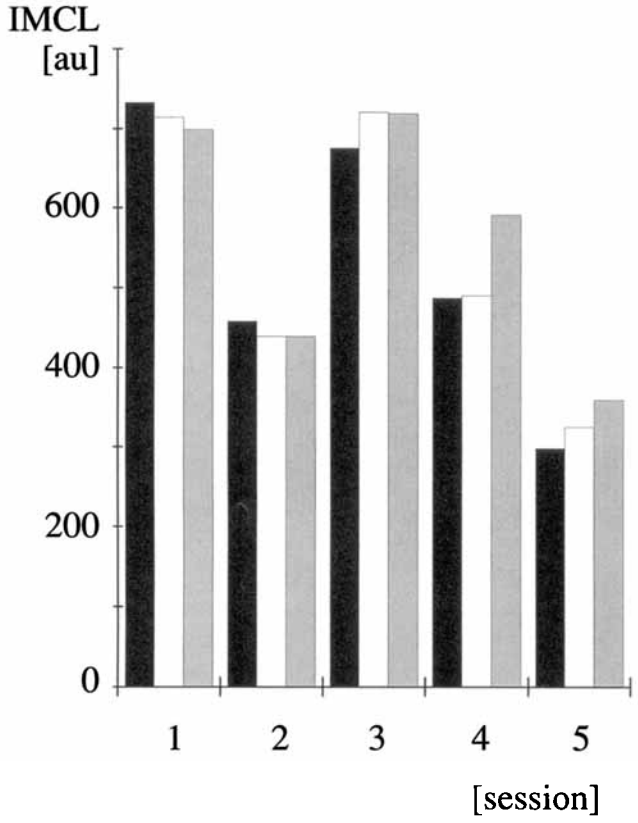

FIG. 7. IMCL levels in repeated measurements in a single subject (female, 24 years) at 5 different days, separated by 1 week each. Before Examinations 2 and 5, the volunteer had hiked for 3 h. Between subsequent IMCL level determinations on the same day, the volunteer left the magnet to make new positioning and parameter optimization necessary. Analysis of variance (Table 1) shows highly significant ($P \ll 0.001$) differences between different days while the residual methodological error within one session is 6.1%.

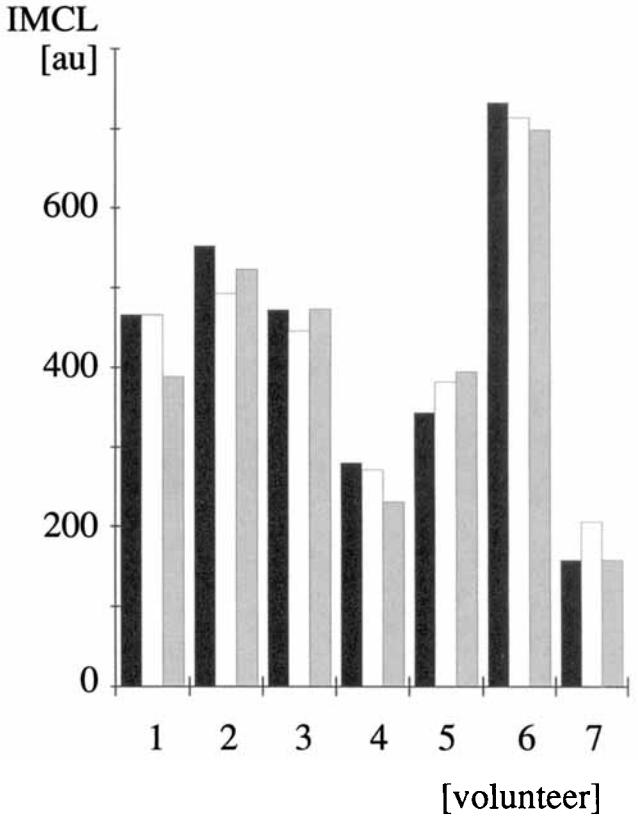

FIG. 8. IMCL levels in arbitrary units in seven different subjects (3 female, 4 male, average age 31 years). Three subsequent measurements were performed on each volunteer. Analysis of variance (Table 1) shows highly significant ($P \ll 0.001$) differences between subjects while the residual methodological error within a single subject is 6.7%.

Recovery

Figure 10 shows the time-resolved recovery of IMCL from strenuous exercise of about 3 h duration in one volunteer. Exercise induced a drop of IMCL of about 40% in the tibialis *anterior* muscle. Interestingly, IMCL recovery did not start immediately post-exercise but several hours later after a meal. IMCL levels increased with a time constant of 40.3 h (corresponding to $t_{1/2}$ of 28 h). In contrast, Cr showed nearly unchanged levels pre-exercise and during recovery. The IMCL recovery overshot the pre-load level, which had been determined repeatedly before the workload.

DISCUSSION

EMCL can be found along muscles in fasciae and in subcutaneous fat layers. This bulk fat is metabolically relatively inert, but capable of supplying a large fraction of substrate mainly during very low intensity exercise (27). IMCL are more accessible for mitochondrial aerobic metabolism and are effectively used at higher work intensities in particular (14, 27). While there has been some controversy over the years about the relative usage of lipids and carbohydrates for energy supply (28), it is generally accepted that lipids can cover up to 70–90% of the substrate needs in long-term exercise (14, 27). There is evidence that glycogen/glucose and lipids complement each other in a reciprocal way (28).

Human muscle contains glycogen at about 72 m*M in vivo* (29) or 350 mmols/kg dry weight (30). The amount of triglycerides in human muscle can vary considerably between 5–60 mmol/kg (14) corresponding to about 0.3 to 0.8 vol % (31). An important clue to the role of IMCL in muscle metabolism is the observation of a close spatial neighborhood of mitochondria and lipid droplets (13), which can also be seen in Fig. 3.

This report demonstrates that ^{1}H-MRS of IMCL is feasible and yields biologically relevant results complementing the noninvasive determination of glycogen by ^{13}C-MR spectroscopy. MRS is therefore a promising tool for the comprehensive investigation of intra-myocellular substrate stores in sports medicine, rehabilitation, and pathology.

Angular Dependence of CH_2-Resonances

CH_2-resonances of lipids in human muscle show two different portions with very distinct angular dependence of the resonance positions (Fig. 4). Starting from the observations of Schick *et al.* (11) who compared lipid resonances from bulk fat and muscle, it is reasonable to

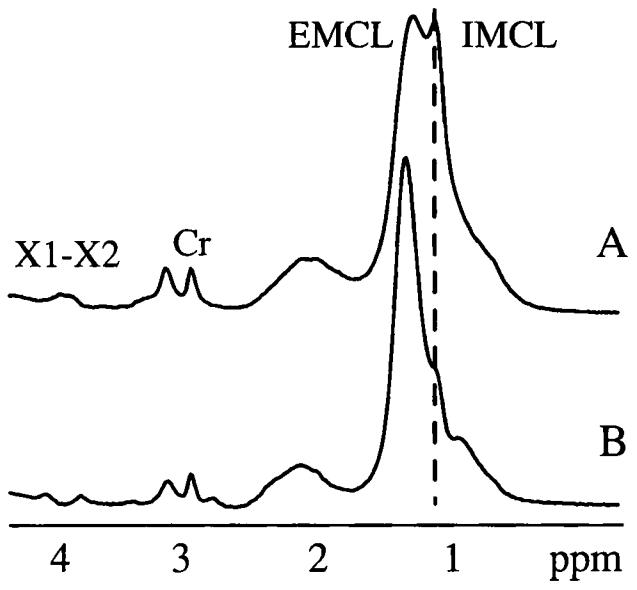

FIG. 9. Comparison of ^{1}H-MR spectra of human gastrocnemius (lower trace) and soleus (upper trace) muscles. Each spectrum represents an average of 8 spectra obtained from 8 male subjects. Soleus muscle obviously contains larger amounts of IMCL (dotted line) compared with gastrocnemius muscle. Differences in the splitting of the X1-X2 doublet (Creatine CH2) in the two muscles are due to dipolar coupling (17, 18) and are caused by the different alignment of the muscle fibers.

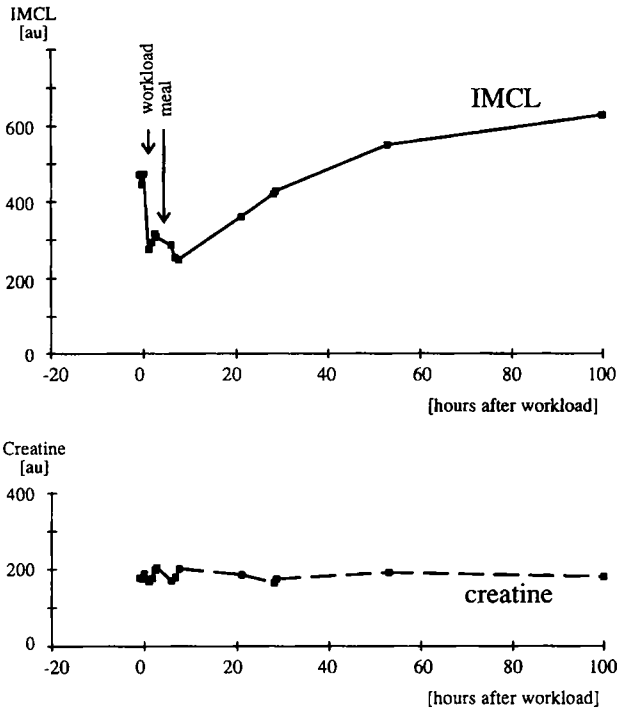

FIG. 10. IMCL levels in arbitrary units in a single volunteer (male, 27 years) after a strenuous exercise (3 h bicycle training at personal maximal limit). Three spectra had been obtained 1 day before the workload. Note that the time points of the preload spectra are arbitrarily set. Within 160 min after workload, IMCL levels were determined four times. After a meal, IMCL levels were again determined eight times over the subsequent 100 h. An exponential fit of the recovery curve (fit beginning 6 h after workload) revealed a time constant of 40.3 h, corresponding to $t_{1/2}$ of 28 h.

hypothesize that the orientation dependence of EMCL signals is due to anisotropic magnetic susceptibility. To estimate and to describe the effect theoretically, it is necessary to idealize the geometry of the spatial distribution of EMCL and IMCL. From Fig. 3 it seems that a sphere is a reasonable approximation of the IMCL droplets. Moreover, we can safely assume that these small spheres are evenly distributed throughout most muscle fibers. According to Eq.[A2] of the Appendix, signals from lipids stored in the form of evenly distributed spheres will not lead to a frequency shift when the leg is rotated in the magnetic field. It seems therefore plausible to assign this resonance to the CH_2-groups of IMCL.

A second signal contribution shows an angular dependent shift and line broadening, which is largest when the leg is perpendicular and smallest when the leg is parallel to the magnet axis (Fig. 4). Eq.[A3] and [A4] of the Appendix explain this behavior by bulk susceptibility given a tube-like geometry. The model of a tube for the distribution of EMCL seems justifiable based on the available macroscopical structural evidence. A corresponding resonance frequency shift of about 0.21 ppm results from this geometry. Methylene signals from bulk fat in layers around muscle tissue oriented parallel to the field is therefore expected to resonate at 1.46 ppm (Eq.[A3]), which is confirmed by the experiment (Fig. 4). The inhomogeneous contribution **I** depends on the exact geometry of the two compartments. It is zero for bulk fat in a concentric tube parallel to the field (Eq.[A3]). This explains the experimental observation that the orientation-dependent line is sharpest under that condition. Bulk susceptibility shifts of fat layers perpendicular to the magnetic field are less predictable since **I** is non-zero (Eq.[A4]) and a function of the exact geometry and relative distances. Even without quantitative evaluation of **I**, the observed line broadening can be predicted qualitatively. Since the model explains both the shift-dependence and the broadening of the signals, the second signal is attributed to EMCL.

From the observation that the two signals are separated best with the muscle parallel to the magnetic field, the experimental setup can be optimized. However, only muscles containing fibers parallel to the main anatomical axis show this optimum separation if the muscle (i.e., the extremity) is parallel to the magnet. Muscles where fibers and limb axis are not parallel (e.g., soleus) will show less separation of the CH_2 signals if extremities are placed parallel to the magnetic field as it is usually done.

Increasing Voxel Size

As second clue for the assignment of the two CH_2 signals is obtained from the experiment where the voxel size was increased stepwise. Figures 5 and 6 show a characteristic behavior for both lipid compartments. While the signal at 1.25 ppm scales with the signals from water and metabolites, the signal at 1.5 ppm is independent of the other resonances and increases steeply as voxel size increases – in particular when the surface of the muscle is reached. The almost perfect correlation of water content in the

voxel with the nominal volume indicates that the volume selection is technically reliable and that the terms "area of the water signal" and "volume of the voxel" are exchangeable. The linear correlations between total metabolite, Cr, and water signals indicate that the voxel contains mostly muscle tissue and that these compounds are evenly distributed within the voxel. The fatty acid signal at 1.25 ppm increases linearly with the water signal, with Cr, and with the sum of the metabolite peaks, i.e., it scales with the volume of muscular tissue. This is best explained by evenly distributed fatty acid droplets in the cytoplasm of muscle cells, i.e., by IMCL. The resonance at 1.5 ppm behaves differently. It is obvious that this signal is not evenly distributed in the voxel, but originates predominantly from fat layers that are included in large voxels only, i.e., which are surrounding the muscle. It can therefore be assigned to EMCL. It should be noted that this signal can dominate the ^{1}H-MR spectrum if voxels are not small enough or are not placed very carefully within a muscle. Precise anatomical localization of a voxel is therefore mandatory for ^{1}H-MRS of muscle (Fig. 1), not only for the detection of IMCL, as shown here, but also for the observation of other orientation-dependent features of the muscle spectrum (17).

Fitting Algorithms

The crucial point for the quantitation of IMCL in human muscle by means of ^{1}H-MRS is the separation of the methyl and various methylene signals of EMCL and IMCL. Beside anatomically correct placement of the voxel as stated above, the accuracy of the IMCL determination can be improved by sophisticated fitting algorithms that allow for incorporation of prior knowledge (22–24) as described in the Methods section. Predefined relations between peak areas, resonance frequencies, linewidths, or phases reduce the number of parameters-to-fit and lead to a lower variance of the estimated parameters. The quality of the fit turned out to be better if the metabolite part of the spectrum was fitted with Lorentzian lines and the IMCL and EMCL signals with Gaussian lines. It has recently been demonstrated (23) that further improvement of fit quality for the EMCL and IMCL part of the spectrum is obtained with Voigt lines, i.e., a time domain product of a Lorentzian and a Gaussian shape. Figure 2 shows that scaled subtraction of *in vivo* spectra can yield almost pure spectra of IMCL or EMCL from which prior knowledge can be obtained. It is noteworthy, that the accuracy of the IMCL determination is improved by sophisticated fitting algorithms, but that even without this data treatment, the main effects, such as IMCL recovery, can be drawn unambiguously from the original spectra. In the presented study, most spectra are obtained from *M. tibialis anterior* representing the optimal experimental situation, because of the parallel alignment of muscle fibers. In other muscles, where fibers may not be oriented parallel to the static field, IMCL may be less well separated from EMCL in the ^{1}H-MR spectrum and an optimal fitting strategy may therefore be mandatory.

Reproducibility

This study shows that IMCL can be determined in *M. tibialis anterior* with a reproducibility of approximately 6%. This precision is similar to that achieved for other MR visible metabolites and is sufficient to allow for quantitative estimates of biologically relevant changes in intra-myocellular lipid concentrations. The agreement between methodological errors as determined from the intra-individual and inter-individual ANOVA test, respectively, indicates that these variations have been extracted properly and that the residual error indeed represents the achievable methodological precision. In addition, it implies that the single subject measured for the determination of intra-individual variations is a representative case for the group studied for inter-individual variation. Two main conclusions can be drawn from the repeated IMCL determinations in humans (Figs. 7 and 8): 1) The amount of IMCL is significantly different between subjects ($P \ll 0.001$). 2) IMCL levels depend strongly on physical activity and may vary significantly within short periods of time ($P \ll 0.001$), while Cr levels remain stable (within 3%). Another explanation for variations of IMCL levels may be recent dietary history (18). Cr levels differ significantly between subjects, too ($P = 0.004$). In the current study, IMCL levels, as determined by ^{1}H-MRS, are expressed in arbitrary units, because the additional measurements needed to convert to absolute units were beyond the scope of this study.

Soleus versus Gastrocnemius

The presented study has almost exclusively been carried out in the parallel-fibered *M. tibialis anterior*. Although the experimental setup for soleus and gastrocnemius muscle was not yet optimized, it is obvious from the data presented in Fig. 9 that individual muscles indeed appear to have very distinct IMCL levels.

Recovery

The results from the preliminary study of recovery after heavy exercise indicate that IMCL can be mobilized within hours and recovered within days. In our volunteer, a time constant of approximately 40 h was determined for recovery, eventually leading to an overshoot. This is considerably shorter than what had been reported for repletion after a marathon run (32), where biopsies revealed a recovery time of many days. However, details of this recovery, including time constant, delay before regeneration and overshoot, may only be characteristic for the particular single experimental setup used. They should not be viewed as statistically significant for general muscle physiology. Nevertheless, the study shows that follow-up in single subjects is technically feasible and demonstrates that individual recovery can be determined with satisfactory accuracy.

Our observation of a $t_{1/2}$ of approximately 28 h for the recovery of IMCL in a single volunteer is somewhat longer than that of glycogen, where for the insulin-independent phase (above 35 m*M*) an approximately linear recovery has been reported with a rate of 3.5 m*M*/h, which would result in about 11 h for restoration from 35 m*M* to resting levels of 72 m*M* (29).

It is striking that the female volunteer in the intra-individual reproducibility study reduced her IMCL levels with low intensity workloads to a similar extent as the male volunteer in the recovery study with a much higher effort. A possible explanation of this supposed discrepancy is offered by the fact that the portion of energy supplied by fatty acids decreases with higher workload while the use of carbohydrates increases (13, 14).

CONCLUSIONS

Up to now, reliable determination of IMCL has only been possible through muscle biopsies (14, 31). The presented study shows that ^{1}H-MRS can be used to determine IMCL levels noninvasively. The separation of the MR signals of EMCL and IMCL is feasible, and IMCL levels can be determined in absolute, but arbitrary units with a reproducibility of about 6–7%. The conversion to standardized units is possible, but will require additional calibration measurements and corrections.

Glycogen and lipids are reciprocal energy supplies for the human body. MRS has the potential to measure both metabolites noninvasively and therefore repeatedly. While glycogen is accessible by means of ^{13}C-MRS, IMCL can be determined by ^{1}H-MRS in the same session. MRS promises therefore to become the method of choice for the investigation of long-term energy storage of the human body in sports medicine and pathology.

APPENDIX

Bulk magnetic susceptibility (BMS) shifts of the resonance-frequency have been calculated by Chu *et al.* (33) for various geometrical shapes. In the following, the definitions and the terminology of these authors are adapted. In a simplified way, two types of lipid accumulations in the muscle can be distinguished: IMCL in droplets with roughly spherical geometry surrounded by cellular water and EMCL in fat layers, which can be characterized by coaxial cylinders, with EMCL in the annular compartment and water on the inside and outside. Figure 11 shows the two cases parallel and perpendicular to the static magnetic field $\mathbf{B}_0$.

Two theoretical contributions to the BMS shift can be distinguished (33): a homogeneous part D and an inhomogeneous contribution $\mathbf{I}$. The field $\mathbf{B}_i$ can be written as (i representing the different compartments):

$$\mathbf{B}_i = \{1 + D_i\}\mathbf{B}_0 + \mathbf{I}_i \qquad [A1]$$

D and $\mathbf{I}$ are functions of the diamagnetic susceptibility of the substances (34) in the different compartments, i.e., water with $X_W = -9.05 \cdot 10^{-6}$, and lipids. Using the composition of free fatty acids in plasma (15) as an estimation for the composition of lipid droplets (24% palmitic acid, 14% stearic acids, 43% oleic acids, and 10% linoleic acids) one can estimate an average $X_L = -8.44 \cdot 10^{-6}$ (34). In addition, $\mathbf{I}$ depends on the exact geometry of the compartment.

The BMS within a lipid sphere is primarily determined by the diamagnetic susceptibility outside the sphere (i.e., X_W) and can be approximated by:

$$D = X_w/3 \text{ and } \mathbf{I} = 0 \qquad [A2]$$

It is obvious that a rotation of a sphere will not change these contributions. However, for infinite coaxial cylinders, the BMS changes with the angle between field and cylinder axis. For a cylinder parallel to the external field $\mathbf{B}_0$, D and $\mathbf{I}$ of the annular lipid compartment can be calculated as:

$$D = X_L/3 \text{ and } \mathbf{I} = 0 \qquad [A3]$$

which is the same as for isotropic bulk fat far from compartmental boundaries. For a cylinder perpendicular to the external field, D and $\mathbf{I}$ become:

$$D = X_W/2 - X_L/6 \text{ and } \mathbf{I} \propto \left\{\frac{\cos 2\theta}{r^2}\right\} \qquad [A4]$$

with r being the radial distance from a nucleus to the axis of the cylinder, and θ being the angle between the external field and r.

If the influence of the inhomogeneous contribution is neglected outside a small sphere – which seems to be reasonable for a small droplet in a much larger muscle – the BMS inside and outside of a sphere is the same, i.e., lipids in a small sphere are expected to resonate at the position of free lipids dissolved in water (1.25 ppm). The difference between BMS within the sphere (Eq. [A2]) and in a tube parallel to the external magnetic field $\mathbf{B}_0$ (Eq. [A3]) is 0.21 ppm, i.e., lipids in a tube parallel to the

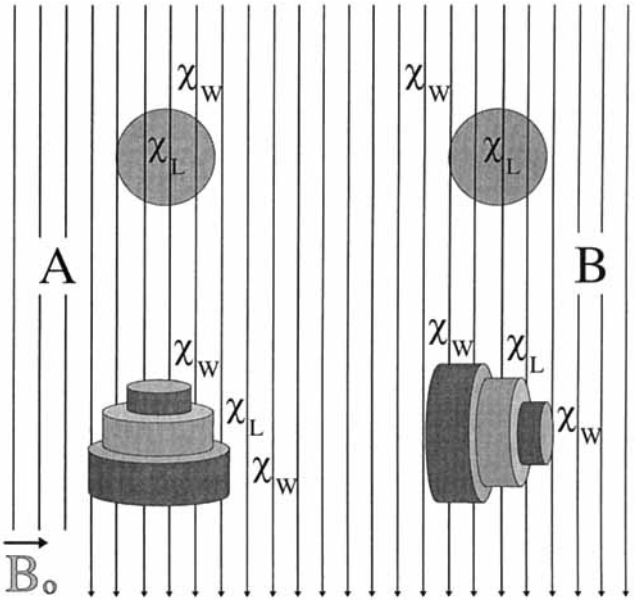

FIG. 11. Comparison of susceptibility effects on spherical and tubular structures at two different angles with respect to the static magnetic field B_0. The left side (A) illustrates the case where muscular fibers are parallel to B_0 (i.e., vertical); the right side (B) shows muscular fibers perpendicular to B_0. While susceptibility effects acting on spherical structures (such as lipid droplets) are independent of the angle between muscle fiber and B_0, tubular structures are subject to anisotropic susceptibility shifts, as described in the Appendix.

magnetic field resonate at 1.46 ppm. The homogeneous contribution D in the case of a tube perpendicular to $\mathbf{B}_0$ (Eq. [A4]) would lead to a resonance frequency of 1.15 ppm for lipids. The angular and radial dependence of the inhomogeneous contribution **I** will lead to a symmetrical distribution of the resonance frequencies resulting in a line broadening. Maximum shifts in either direction are reached when the static magnetic field is parallel or perpendicular to the lipid layer.

ACKNOWLEDGMENTS

The authors thank H.Claassen and R.Vock for providing the EM image.

REFERENCES

1. B. Chance, Noninvasive approaches to oxygen delivery and cell bioenergetics in functioning muscle. *Clin. J. Sport Med.* **2,** 132–138 (1992).
2. M. L. Blei, K. E. Conley, M. J. Kushmerick, Separate measures of ATP utilization and recovery in human skeletal muscle. *J. Physiol.* **465,** 203–222 (1993).
3. G. J. Kemp, G. K. Radda, Quantitative interpretation of bioenergetic data from 31P and 1H magnetic resonance spectroscopic studies of skeletal muscle: An analytical review. *Magn. Reson. Q.* **10,** 43–63 (1994).
4. J. A. Kent-Braun, R. G. Miller, M. W. Weiner, Magnetic resonance spectroscopy studies of the human muscle. *Radiol. Clin. North Am.* **32,** 313–335 (1994).
5. M. J. Avison, D. L. Rothman, E. Nadel, R. G. Shulman, Detection of human muscle glycogen by natural abundance 13C NMR. *Proc. Natl. Acad. Sci. USA* **85,** 1634–1636 (1988).
6. S. R. Williams, D. G. Gadian, E. Proctor, D. B. Sprague, D. F. Talbot, I. R. Young, F. F. Brown, Proton NMR studies of muscle metabolites in vivo. *J. Magn. Reson.* **63,** 406–412 (1985).
7. P. A. Narayana, J. D. Hazle, E. F. Jackson, L. K. Fotedar, M. V. Kulkarni, In vivo 1H spectroscopic studies of human gastrocnemius muscle at 1.5 T. *Magn. Reson. Imaging* **6,** 481–485 (1988).
8. M. Barany, P. N. Venkatasubramanian, Volume-selective water-suppressed proton spectra of human brain and muscle in vivo. *NMR Biomed.* **2,** 7–11 (1989).
9. H. Bruhn, J. Frahm, M. L. Gyngell, K. D. Merboldt, W. Haenicke, R. Sauter, Localized proton NMR spectroscopy using stimulated echoes: applications to human skeletal muscle in vivo. *Magn. Reson. Med.* **17,** 82–94 (1991).
10. J. W. Pan, J. R. Hamm, H. P. Hetherington, D. L. Rothman, R. G. Shulman, Correlation of lactate and pH in human skeletal muscle after exercise by ^{1}H NMR. *Magn. Reson. Med.* **20,** 57–65 (1991).
11. F. Schick, B. Eismann, W. I. Jung, H. Bongers, M. Bunse, O. Lutz, Comparison of localized proton NMR signals of skeletal muscle and fat tissue in vivo: two lipid compartments in muscle tissue. *Magn. Reson. Med.* **29,** 158–167 (1993).
12. S. R. Kayar, H. Hoppeler, H. Howald, H. Claassen, F. Oberholzer, Acute effects of endurance exercise on mitochondrial distribution and skeletal muscle morphology. *Eur. J. Appl. Physiol.* **54,** 578–584 (1986).
13. R. Vock, H. Hoppeler, H. Claassen, D. X. Y. Wu, J. M. Weber, C. R. Taylor, E. R. Weibel, Design of the oxygen and substrate pathways. VI. Structural basis of intra-cellular substrate supply to mitochondria in muscle cell. *J. Exp. Biol.*, **199,** 1689–1697 (1996).
14. F. Oberholzer, H. Claassen, H. Moesch, H. Howald, Ultrastrukturelle, biochemische und energetische Analyse einer extremen Dauerleistung (100 km-Lauf). *Schweiz. Z. Sportmed.* **2,** 71–98 (1976).
15. R. J. Havel, L. A. Carlson, L. G. Ekelund, A. Holmgren, Turnover rate and oxidation of different free fatty acids in man during exercise. *J. Appl. Physiol.* **19,** 613–618 (1964).
16. R. Gruetter, T. A. Prolla, R. G. Shulman, ^{13}C NMR visibility of rabbit muscle glycogen in vivo. *Magn. Reson. Med.* **20,** 327–332 (1991).
17. R. Kreis, C. Boesch, Liquid-crystal-like structures of human muscle demonstrated by in vivo observation of direct dipolar coupling in localized proton magnetic resonance spectroscopy. *J. Magn. Reson. Series B* **104,** 189–192 (1994).
18. R. Kreis, M. Koster, M. Kamber, H. Hoppeler, C. Boesch, In vivo spectroscopy at the magic angle and creatine supplementation for the elucidation of ^{1}H-MR spectra of human muscle, *in* "Proc., SMR, 3rd Annual Meeting, Nice, 1995," p. 430.
19. C. Boesch, H. Slotboom, A. Puntschart, H. Hoppeler, R. Kreis, Measurement of intra-myocellular lipid-signals in ^{1}H-MR-spectra of human muscle in vivo, *in* "Proc., SMR, 3rd Annual Meeting, Nice, 1995," p. 426.
20. P. A. Bottomley, U.S. Patent 4,480,228 (1984).
21. J. Hennig, The application of phase rotation for localized in vivo proton spectroscopy with short echo times. *J. Magn. Reson.* **96,** 40–49 (1992).
22. J. Slotboom, B. A. P.M. Vogels, J. G. deHaan, J. H. N. Creyghton, G. Quack, R. A. F. M. Chamuleau, W. M. M. J. Bovee, Proton resonance spectroscopy study of the effects of L-Ornithine-L-Aspartate on the development of encephalopathy, using localization pulses with reduced specific absorption rate. *J. Magn. Reson. Series B* **105,** 147–156 (1994).
23. J. Slotboom, R. Kreis, C. Boesch, Frequency domain fitting using time domain models and prior knowledge, *in* "Proc., ISMRM, 4th Annual Meeting, New York, 1996," p.1188.
24. A. A. deGraaf, W. M. M. J. Bovee, Improved quantification of in vivo ^{1}H NMR spectra by optimization of signal acquisition and processing and by incorporation of prior knowledge into the spectral fitting. *Magn. Reson. Med.* **15,** 305–319 (1990).
25. R. Kreis, T. Ernst, B. D. Ross, Absolute quantitation of water and metabolites in the human brain. II. Metabolite concentrations. *J. Magn. Reson. Series B* **102,** 9–19 (1993).
26. P. Armitage, G. Berry, "Statistical Methods in Medical Research," Blackwell Scientific Publications, Oxford, UK, 1994.
27. J. A. Romijn, E. F. Coyle, L. S. Sidossis, A. Gastaldelli, J. F. Horowitz, E. Endert, R. R. Wolfe, Regulation of endogenous fat and carbohydrate metabolism in relation to exercise intensity and duration. *Am. J. Physiol.* **265,** E380–E391 (1993).
28. G. A. Brooks, J. Mercier, Balance of carbohydrate and lipid utilization during exercise: the "crossover" concept. *J. Appl. Physiol.* **76,** 2253–2261 (1994).
29. T. B. Price, D. L. Rothman, R. Taylor, M. J. Avison, G. I. Shulman, R. G. Shulman, Human muscle glycogen resynthesis after exercise: insulin-dependent and independent phases. *J. Appl. Physiol.* **76,** 104–111 (1994).
30. R. C. Harris, E. Hultman, L. O. Nordesjo, Glycogen, glycolytic intermediates and high-energy phosphates determined in biopsy samples of musculus quadriceps femoris of man at rest. Methods and variance of values. *Scand. J. Clin. Lab. Invest.* **33,** 109–120 (1974).
31. H. Hoppeler, P. Lüthi, H. Claassen, E. R. Weibel, H. Howald, The ultrastructure of the normal human skeletal muscle. A morphometric analysis on untrained men, women, and well-trained orienteers. *Pflugers Arch.* **344,** 217–232 (1973).
32. R. S. Staron, R. R. Hikida, T. F. Murray, F. C. Hagerman, M. T. Hagerman, Lipid depletion and repletion in skeletal muscle following marathon. *J. Neurol. Sci.* **94,** 29–40 (1989).
33. S. C. K. Chu, J. A. Balschi, C. S. Springer, Bulk magnetic susceptibility shifts in NMR studies of compartmentalized samples: use of paramagnetic reagents. *Magn. Reson. Med.* **13,** 239–262 (1990).
34. D. R. Lide, "Handbook of Chemistry and Physics," 74th ed., CRC Press, Boca Raton, FL, 1993.